J Therm Anal Calorim (2012) 108:807–815
DOI 10.1007/s10973-011-2050-3

Hepta isobutyl polyhedral oligomeric silsesquioxanes (hib-POSS)

A thermal degradation study

I. Blanco · L. Abate · F. A. Bottino · P. Bottino

MEDICTA2011 Conference Special Chapter

Abstract Six polyhedral oligomeric silsesquioxanes (POSSs) with general formula R_7 R'_1 $(SiO_{1.5})_8$, where R- was an isobutyl group and R′- a variously substituted phenyl group, namely hepta isobutyl polyhedral oligomeric silsesquioxane (hib-POSS), were prepared and their composition was checked by elemental analysis and ^1H NMR spectroscopy. The degradation of compounds obtained was studied by simultaneous differential thermal analysis/thermogravimetry (DTA/TG) technique, in both inert (flowing nitrogen) and oxidative (static air atmosphere) environments, in order to draw useful information about their thermal stability. Experiments, performed in the 35–700 °C temperature range, showed different behaviour between the two used atmospheres. The formation of volatile compounds only, with an about complete mass loss, was observed under nitrogen, while a solid residue (≈40–50% in every case), due to the formation of SiO_2, as indicated by the FTIR spectra, was obtained in static air atmosphere. The results obtained were discussed and compared, and the classifications of resistance to thermal degradation in the studied environments were made. A comparison between the thermal stabilities of hib-POSSs and analogous cyclopentyl POSSs previously studied was also performed.

Keywords POSS · Silsesquioxanes · Thermal degradation · Thermogravimetric analysis

I. Blanco (✉) · L. Abate · F. A. Bottino
Department of Industrial and Mechanical Engineering, University of Catania, V.le A. Doria 6, 95125 Catania, Italy
e-mail: iblanco@dmfci.unict.it

P. Bottino
Department of Pharmaceutical Sciences, University of Catania, V.le A. Doria 6, 95125 Catania, Italy

Introduction

Polymer nanocomposites are a novel class of materials formed through the dispersion at nanoscale level of an inorganic compound in a polymer.

The major reason of interest in introducing inorganic structures into polymers at nanoscale level is the enhancement in physical, mechanical, barrier, and flammability properties in comparison with those of virgin polymer and conventionally filled polymer composites [1]. In addition, nanocomposites exhibit a pronounced increase in thermal stability [2–4], which is important because they can be subjected to high temperatures during processing or in service.

Various nanoparticles, such as carbon nanotubes, layered silicates, etc., have been used in the past to prepare organic–inorganic hybrid systems [5–14], but, in the last years, another class of nanoparticles, polyhedral oligomeric silsesquioxanes (POSSs), has awaken an increasing interest for the formulation of nanocomposites [15–21].

A typical POSS nanoparticle is formed by an inorganic Si_8O_{12} nanostructured skeleton surrounded by eight organic groups, such as alkyl, aryl or any of their derivatives, linked to silicon atoms by covalent bonds [22, 23]. POSSs are thus hybrid inorganic/organic materials with formula $(RSiO_{1.5})n$, or R_nT_n, where organic substituents (R), which can be the same or different, are attached to a silicon–oxygen cage (T).

The most common molecular formulas of POSSs are $(RSiO_{1.5})_8$ or $R_7R'_1(SiO_{1.5})_8$. The nature of R- and R′- affects the solubility in conventional solvents, the compatibility with polymers and the capability to undergo nanometric dispersion in host polymer matrices, and then the thermal, physical, and mechanical properties of the resulting nanocomposites. In particular, on the basis of recent studies on

homosubstituted POSSs of type $(RSiO_{1.5})_8$, were R- is an alkyl (C_2–C_{10}) chain, the presence of aliphatic groups appears to increase solubility but to worsen thermal properties [24–26]. By contrast, the presence of aromatic groups seems to act in the opposite direction, considerably enhancing thermal stability but decreasing solubility and compatibility [27].

Due to the relevant and increasing technological importance of POSSs, our group has planned a wide research programme on the synthesis and characterization of variously substituted POSSs, aiming to obtain compounds with high thermal stability coupled with sufficiently good compatibility and solubility in polymer matrix, to be used in the preparation of new thermally stable nanocomposites having polystyrene (PS) and polyolefins as matrices.

In the first part of this research some $R_7R'_1(SiO_{1.5})_8$ POSSs, where R = cyclopentyl and R′ = mono-, di- or trisubstituted phenyl group, were synthesized and their thermal stabilities were determined and compared [28]. The results obtained were encouraging because all compounds showed high thermal stability, thus suggesting the possibility of their use also in quite drastic conditions.

On continuing our research, in this work we synthesized a new series of POSSs of general formula $R_7R'_1(SiO_{1.5})_8$, where R = isobutyl and R′ = mono- or di-substituted phenyl group, the substituents present in R′- being the same of those in the quoted cyclopentyl derivatives (Fig. 1). The isobutyl group was selected because it is known in literature that a POSS molecule with an isobutyl periphery has a diameter of approximately 1.5 nm [29], thus giving rise to well-dispersed nanocomposites and then ensuring good compatibility with polymer matrix. In addition, due to the simple route of preparation and to the low cost, the hepta isobutyl polyhedral oligomeric silsesquioxanes (hib-POSSs) here studied appear attractive for the use as nanofillers in the production of nanocomposites.

The obtained hib-POSSs were characterized by elemental analysis and ^1H NMR spectroscopy. Thermogravimetric (TG) and differential thermogravimetric (DTG) analysis, differential thermal analysis (DTA) and differential scanning calorimetry (DSC) experiments were then carried out to investigate the thermal behaviour of the studied compounds in both inert and oxidative atmospheres, and to verify if and how much their thermal stability changed on changing substituent on the aromatic ring. To this aim the results obtained for the various compounds were compared with each other, and, also, with those of cyclopentyl derivatives (CP-POSSs) previously studied [28], in order to investigate how the substitution of cyclopentyl groups with isobutyl linked to silicon-oxygen cage affects thermal stability.

Experimental

Materials

Isobutyltrimethoxysilane and phenyltrimethoxysilane have been purchased from Aldrich Co. and used as received. 4-Fluorophenyltrimethoxysilane, 2,4-difluorophenyltrimethoxysilane, 4-methylphenyltrimethoxysilane, xyliltrimethoxysilane and 4-methoxyphenyltrimethoxysilane were prepared from the appropriate Grignard reagent and $Si(OCH_3)_4$ [30–33]. The isobutyltrisilanol $(iC_4H_9)_7$–Si_7O_9 $(OH)_3$ was prepared according to literature methods [34]. Tetrahydrofuran was distilled over a Na-benzophenone mixture.

Compounds **1**–**6** were prepared by Corner Capping Reaction of isobutyltrisilanol with the suitable aryltrimethoxysilane. The same procedure was used for all compounds. The synthesis of **2** is given as an example.

Isobutyltrisilanol (3.95 g, 5.0 mmol) was dissolved in 50 ml of ethanol and *p*-tolyltrimethoxysilane (1.10 g, 5.2 mmol) and 2.0 ml of tetramethylammonium hydroxide were added under stirring. The clear solution was stirred at

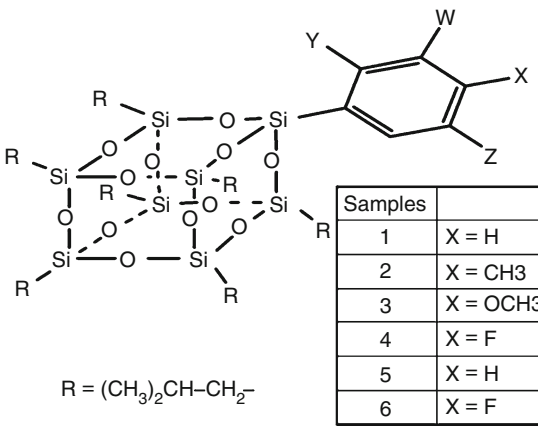

Samples	Substituents			
1	X = H	Y = H	Z = H	W = H
2	X = CH3	Y = H	Z = H	W = H
3	X = OCH3	Y = H	Z = H	W = H
4	X = F	Y = H	Z = H	W = H
5	X = H	Y = H	Z = CH3	W = CH3
6	X = F	Y = F	Z = H	W = H

Fig. 1 Molecular structure of hib-POSSs

room temperature for 24 h. The resulting solid was filtered and washed with two portions (10 ml) of anhydrous ethanol. After drying under reduced pressure, the white solid obtained was crystallized from THF/MeCN mixture to give 3.60 g of desired compound (79.5% yield).

Yield, ^1H NMR spectroscopy and elemental analysis

^1H NMR spectra were recorded on a Varian Unity Inova instrument (^1H 500 MHz) in $CDCl_3$ as solvent. Chemical shifts are in ppm (δ) from TMS as internal standard.

The ^1H NMR data found for the various compounds investigated were the following:

Compound ***1***

Yield 90.3%. ^1H NMR: 7.65 (dd, 2H), 7.42 (dd, 1H), 7.36 (dd, 2H), 1.87 (m, 7H), 0.96 (m, 42 H), 0.63 (m, 14H). Anal. Calcd for $C_{34}H_{68}Si_8O_{12}$: C 45.73, H 7.68. Found: C 45.47, H 7.75.

Compound ***2***

Yield 87.9%. ^1H NMR: 7.55 (d, 2H), 7.18 (d, 2H), 2.36 (s, 3H), 1.86 (m, 7H), 0.96 (m, 42 H), 0.63 (m, 14H). Anal. Calcd for $C_{35}H_{70}Si_8O_{12}$: C 46.35, H 7,78. Found: C 46.11, H 7.81.

Compound ***3***

Yield 84.6%. ^1H NMR: 7.58 (d, 2H), 6.90 (d, 2H), 3.82 (s, 3H), 1.87 (m, 7H), 0.97 (m, 42 H), 0.64 (m, 14H). Anal. Calcd for $C_{35}H_{70}Si_8O_{13}$: C 45.55, H 7.64. Found: C 45.31, H 7.71.

Compound ***4***

Yield 80.5%. ^1H NMR: 7.65 (dd, 2H), 7.04 (dd, 2H), 1.86 (m, 7H), 0.96 (m, 42 H), 0.63 (m, 14H). Anal. Calcd for $C_{34}H_{67}FSi_8O_{12}$: C 44.88, H 7.41. Found: C 44.62, H 7.48.

Compound ***5***

Yield 69.3%. ^1H NMR: 7.27(s, 2H), 7.06 (s, 1H), 2.31 (s, 6H), 1.87 (m, 7H), 0,97 (m, 42 H), 0.63 (m, 14H). Anal. Calcd for $C_{36}H_{72}Si_8O_{12}$: C 46.95, H 7.88. Found: C 46.79, H 7.93.

Compound ***6***

Yield 61.0%. ^1H NMR: 7.54 (dd, 1H), 6.87 (dd, 1H), 6.76 (dd, 1H), 1.85 (m, 7H), 0.97 (m, 42 H), 0.62 (m, 14H). Anal. Calcd for $C_{34}H_{66}F_2Si_8O_{12}$: C 43.96, H 7.16. Found: C 43.72, H 7.18.

IR spectroscopy

The Fourier Transform Infrared (FTIR) absorption spectra were recorded by a Perkin Elmer model Spectrum 100 spectrometer, using an universal ATR sampling accessory. Spectra were recorded from 4000 to 400 cm^{-1} with a resolution of 2.0 cm^{-1}. The results are an average of three experimental run to test the results reproducibility. Analysis was performed at room temperature, directly on the compound, without any preliminary treatments.

Thermal analysis

A Shimadzu DTG-60 simultaneous DTA–TG apparatus was used for both TG and DTA. Temperature, heat flow and weight calibrations were performed following the procedure reported in the instruction manual of equipment [35] using as standard materials: indium (NIST SRM 2232), tin (NIST SRM 2220) and zinc (NIST SRM 2221a) for temperature; indium (NIST SRM 2232) for heat flow and a set of exactly weighed samples supplied by Shimadzu for the weight. All calibrations of equipment were repeated every 2 weeks.

Scannings were carried out in the temperature range 35–700 °C, at the heating rate of 10 °C min^{-1}, under flowing nitrogen (0.02 L min^{-1}) and in a static air atmosphere. Samples of about 6×10^{-3} g, placed in a 40 μL platinum open pan, were used for experiments. For TG the sample weight as a function of temperature was monitored and recorded by a PC connected with the DTG-60 apparatus. At the end of each run the experimental data were used to plot the percentage of undegraded sample W/W_o% as a function of temperature, where W_o and W were the weights of sample at the starting point and during scanning, respectively. For DTA analysis, the heat flow of sample was monitored and recorded by the PC connected with the DTG-60 apparatus, in order to evaluate enthalpy and temperature of the observed phase transitions.

DSC measurements

A Mettler DSC 20 differential scanning calorimeter, coupled with a Mettler TC 10A processor as control and evaluation unit, was used for heating–cooling–reheating thermal cycles. The enthalpy and temperature calibrations of our apparatus were made, according to the procedure suggested by the manufacturer [36], through two built-in programs which use indium for the enthalpy calibration and the melting points of three metals such as indium, lead and zinc, for that of temperature. The calibration of

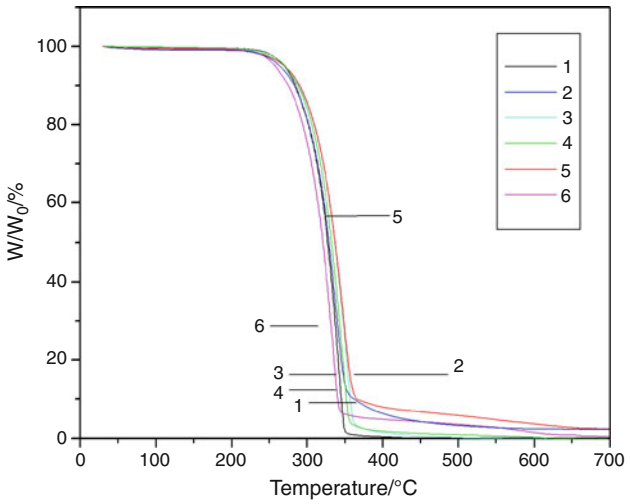

Fig. 2 TG curves under nitrogen flow of differently substituted hib-POSSs

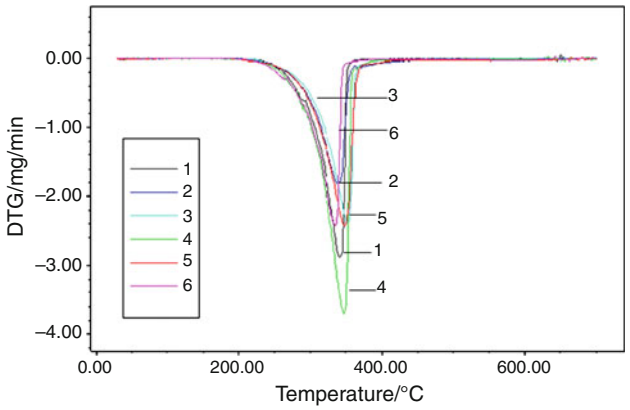

Fig. 3 DTG curves under nitrogen flow of differently substituted hib-POSSs

enthalpy was thus checked by the melting of fresh indium, showing an agreement with the literature standard value [37] within 0.25%, while the accuracy of temperature, checked by several scans with fresh indium and tin, was within 0.08% in respect to literature data [37]. The calibrations were repeated every 2 weeks. Samples of about 6.0×10^{-3} g, held in sealed aluminium crucibles, a heating rate of 10 °C min^{-1} and a nitrogen flow (0.02 L min^{-1}) were used for measurements.

Results and discussion

The thermal behaviour of our compounds was studied by DTA–TG experiments, in dynamic heating conditions, in both inert (flowing nitrogen) and oxidative (static air atmosphere) environments. For all investigated compounds a different behaviour between the used experimental conditions was observed.

The TG and DTG curves under nitrogen (Figs. 2, 3, respectively) evidenced for all hib-POSSs studied, in the complete scanned temperature interval (35–700 °C), a single thermal process falling, in every case, in the 200–400 °C temperature range, with about complete mass loss (≥98%). The initial decomposition temperatures (T_i) were obtained by the TG curves as the intersection between the starting mass line and the maximum gradient tangent to the TG curve. The T_i values under nitrogen are reported in Table 1 together with the temperatures of DTG peaks (T_m), which represent the temperatures at maximum weight loss rate, and the values of the residues obtained after complete temperature scan.

The DTA curves, simultaneously obtained together with the TG and DTG ones, evidenced for all hib-POSSs investigated an endothermic peak, attributable to melting, roughly falling for all compounds in the 200–300 °C temperature range (Fig. 4). This behaviour was confirmed by the visual observation of phenomenon into an equipment for melting point determination (room temperature—300 °C) which showed that a solid–liquid transition occurs for all investigated hib-POSSs in the same temperature interval.

In order to further confirm the occurrence of melting phenomenon, heating–cooling–reheating thermal cycles were then carried out on the studied compounds into our

Table 1 Initial decomposition temperatures (T_i), temperatures at maximum rate of weight loss (T_m) for the main degradation stage and residue% of the studied hib-POSSs in flowing nitrogen and in static air atmosphere

Compound	Nitrogen flow			Air static atmosphere		
	T_i/°C	T_m/°C	Residue%	T_i/°C	T_m/°C	Residue%
1	291.3	341.4	0	235.8	n.d.	52.4
2	285.7	330.4	2.2	242.7	n.d	50.0
3	301.2	353.8	0	263.9	n.d	41.9
4	292.8	336.6	0	232.6	n.d	39.9
5	299.6	348.5	2.0	256.0	n.d	43.3
6	284.9	335.2	0.5	230.7	n.d	47.5

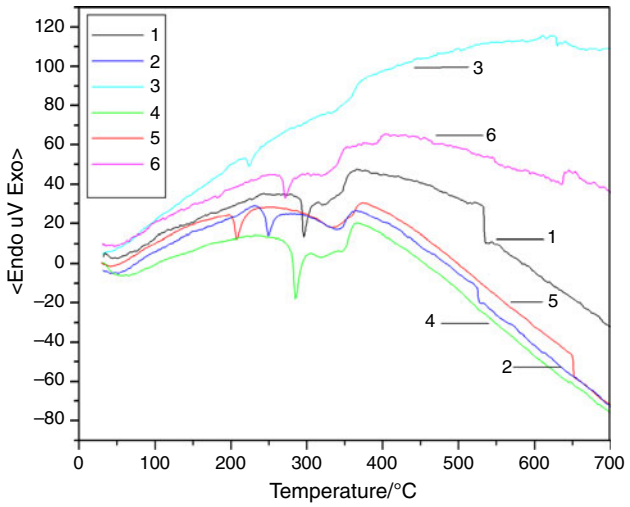

Fig. 4 DTA curves under nitrogen flow of differently substituted hib-POSSs

Table 2 Onset temperature (T_{onset}) and temperature of DTA peak (T_p) of the studied hib-POSSs in flowing nitrogen and in static air atmosphere

Compound	Nitrogen flow		Air static atmosphere	
	T_{onset}/°C	T_p/°C	T_{onset}/°C	T_p/°C
1	292.5	295.9	221.6	243.7
2	235.5	250.0	214.6	277.7
3	217.5	224.1	209.2	290.5
4	273.6	284.8	219.0	241.7
5	199.5	207.8	197.8	207.9
6	268.0	271.5	219.8	236.0

differential scanning calorimeter. To this aim every sample was heated into a pan of equipment up to the end of DSC peak. Onset (T_{onset}) and peak (T_p) temperatures, as well as the associated ΔH values, were determined (Table 3). The obtained T_{onset} and T_p values were in quite satisfactory agreement with those from DTA experiments reported in Table 2. Samples were thus cooled to room temperature and then re-heated twice, and T_{onset}, T_p and ΔH values were again determined after each scan (Table 3). A very good reproducibility (±0.5 °C) was found for both T_{onset} and T_p temperatures, thus indicating the reversibility of considered processes and substantially confirming that the endothermic peaks observed are due to the melting of the studied hib-POSSs. By contrast, relatively little differences were found for enthalpy, which decreased after every thermal cycle. These results indicated that the melting of our compounds was accompanied by evaporation, which continued up to about complete mass loss on increasing temperature, as shown by the TG curves. This finding appears also in agreement with literature results on octaisobutyl POSS [26].

The degradation TG curves of our hib-POSSs in static air atmosphere (Fig. 5) evidenced a different behaviour in respect to nitrogen environment. A very complex degradation process, characterized by several unresolvable stages, was observed, as evidenced by strongly irregular DTG curves, which, due to this reason, do not allow to single out the temperatures at maximum weight loss rate of the degradation processes of various studied compounds, and then are not here reported.

Also, a substantial solid residue was obtained after the complete temperature scan (35–700 °C), which appears due to the formation of SiO_2 as confirmed by the IR spectra which were also performed. This finding is in agreement with our previous results on CP-POSSs [29] and with literature reports on similar compounds [26, 27].

The initial decomposition temperatures and residue% values of the studied silsesquioxanes in static air atmosphere are reported in Table 1. The IR spectrum of the solid residue from compound **6** is reported, as an example, in Fig. 6.

The DTA curves (Fig. 7) confirmed the very complex degradation process in oxidative environment just observed by TG and DTG experiments. It is worth to note that all curves showed a peak in the temperature range 200–270 °C, which was more or less exothermic for the

Table 3 Onset temperature (T_{onset}), peak temperature (T_p), and enthalpy ($-\Delta H$) of fusion from DSC thermal cycles of the studied hib-POSSs in flowing nitrogen

Compound	First heating scan			Second heating scan			Third heating scan		
	T_{onset}/°C	T_p/°C	$-\Delta H$/(J g^{-1})	T_{onset}/°C	T_p/°C	$-\Delta H$/(J g^{-1})	T_{onset}/°C	T_p/°C	$-\Delta H$/(J g^{-1})
1	286.4	291.9	−38.6	286.6	291.9	−37.4	286.0	292.0	−36.0
2	233.0	242.9	−19.3	233.4	242.4	−18.0	233.1	242.7	−17.2
3	214.2	221.1	−20.9	214.4	221.2	−19.7	214.2	221.0	−19.0
4	274.3	282.2	−32.6	274.1	282.1	−31.7	274.3	282.1	−30.8
5	198.8	203.9	−20.1	198.4	203.4	−18.7	198.6	203.4	−16.5
6	261.8	269.9	−30.1	262.0	270.1	−27.8	261.7	270.1	−27.5

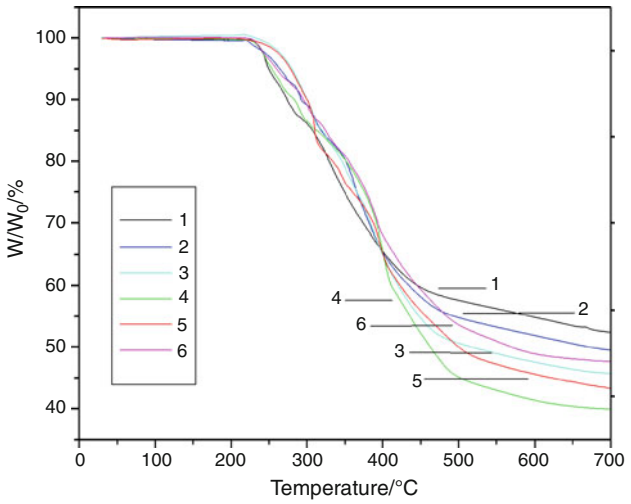

Fig. 5 TG curves in static air atmosphere of differently substituted hib-POSSs

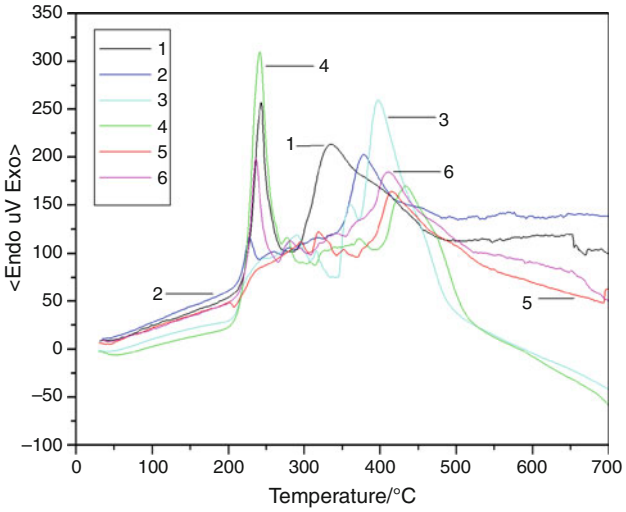

Fig. 7 DTA curves in static air atmosphere of differently substituted hib-POSSs

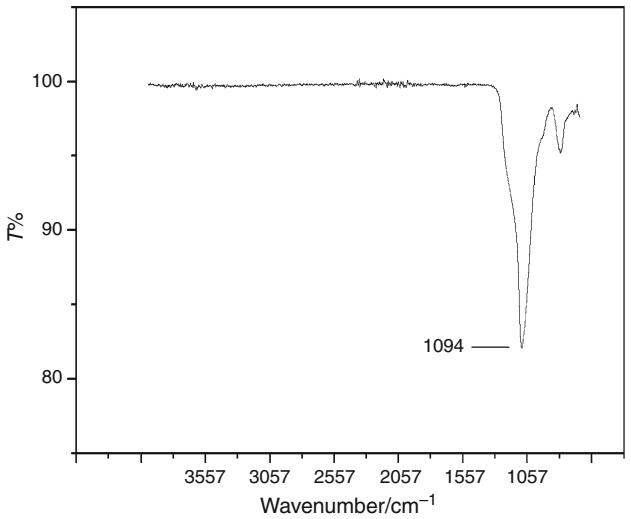

Fig. 6 FTIR spectrum of the residue of compound **5** after thermal degradation in static air atmosphere

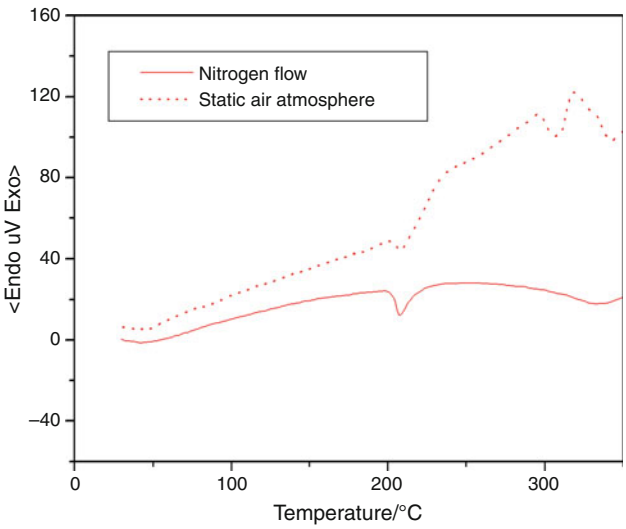

Fig. 8 DTA curves in nitrogen flow and static air atmosphere of compound **5**

compounds **1**, **2**, **3**, **4** and **6** and endothermic for the compound **5**.

On considering the melting temperatures of our compounds (Table 3), this result suggests the occurrence of an exothermic oxidative degradation which precedes or overlaps the melting process. This is in agreement with literature data concerning the degradation of POSSs in oxidative atmosphere [26] as well as with our previous finding on CP-POSSs [29] and it is also supported by the comparison between the DTA curves of each compound in nitrogen and in air. Compound **5**, which is that showing the most low temperature of fusion, evidences in both DTA curves (Fig. 8) the same endothermic peak due to melting (T_p = 207.8 °C under nitrogen; T_p = 207.9 °C in static air atmosphere), immediately followed, only in oxidative environment, by irregular peaks due to oxidative degradation at higher temperatures. Nevertheless, it is important to note that the peak in air is not closed because of the start of decomposition process.

An analogous comparison between the DTA curves of compound **3** (Fig. 9) shows that melting occurs at about the same temperature of initial decomposition process, so a shoulder at T = 244.7 °C, immediately followed by a broad exothermic peak (T_p = 290.5 °C), due to the overlapping of the two processes, is observed in the curve in air.

For the compounds **1**, **2**, **4** and **6**, which show the most high temperatures of fusion, oxidative decomposition precedes the melting process and a sharp exothermic peak in

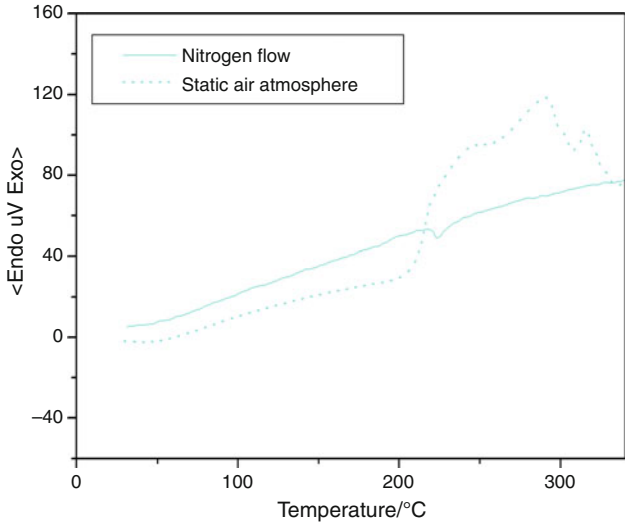

Fig. 9 DTA curves in nitrogen flow and static air atmosphere of compound **3**

the 200–270 °C temperature interval is present in the DTA curves in static air atmosphere, while the endothermic peak due to melting does not appear. The DTA curves of compounds **1**, **2**, **4** and **6**, in both environments are reported in Fig. 10.

Heating–cooling–reheating thermal cycles were then carried out by our DSC equipment also in static air atmosphere, but no reproducibility of T_{onset} and T_p values was observed, it being in agreement with the results over reported.

Some considerations are possible on the results obtained: the initial decomposition temperatures of our hib-POSSs in flowing nitrogen were higher than those in static air atmosphere, thus meaning lower resistance to thermal degradation in oxidative environment.

Appreciable, even though not very large, differences among the T_i values of the various compounds examined in the same environment were found, which were higher in air than under nitrogen. On the basis of the values under nitrogen a classification of the resistance of compound to thermal degradation was made (**3** > **5** > **4** > **1** > **2** > **6**), which was similar to that in air (**3** > **5** > **2** > **1** > **4** > **6**). A further consideration appears opportune: to compare the thermal stability of various compounds it is necessary to take into account not only the initial decomposition temperature, which, in our opinion, is a measure of the resistance of compound to thermal degradation, but, also, the degradation rate. This last parameter is more relevant than the first one when the initial decomposition temperatures of the compounds compared are close with each other.

Since the $(T_m - T_i)$ difference can be considered a measure of the degradation rate, we evaluated these differences by the data in Table 1 for the experiments under nitrogen atmosphere. On the basis of the results obtained the compound **3**, which shows the most high T_i and $(T_m - T_i)$ values, appears the most thermally stable among the investigated hib-POSSs. Analogous considerations were not possible for the data in static air atmosphere, due to the impossibility to determine T_m values.

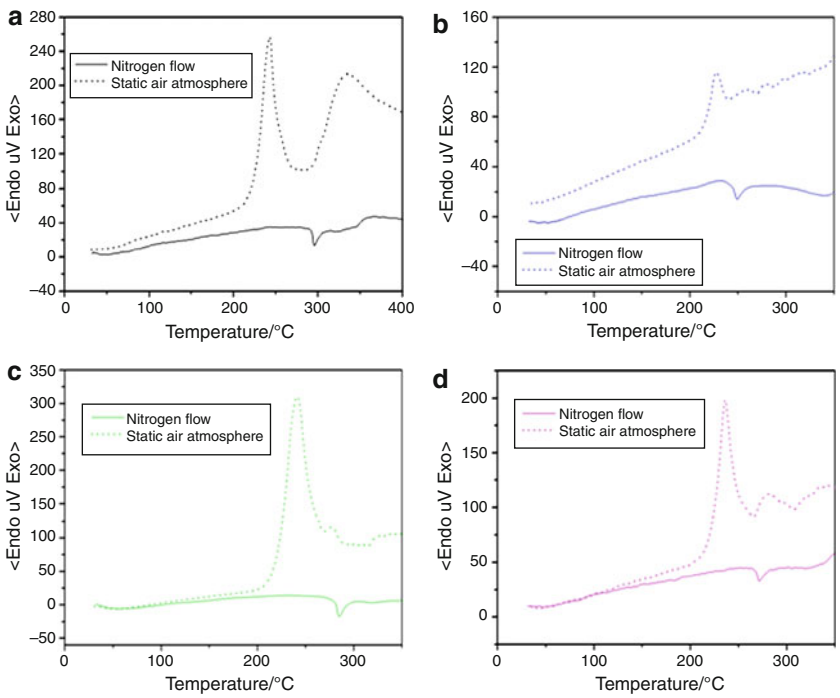

Fig. 10 DTA curves in nitrogen flow and static air atmosphere of compounds: **1** (**a**), **2** (**b**), **4** (**c**) and **6** (**d**)

Conclusions

The results obtained indicate a lesser thermal stability of the hib-POSSs here studied in comparison with the corresponding hepta cyclopentyl polyhedral oligomeric silsesquioxanes previously investigated [29], not only for the lower starting point of decomposition, but also from the point of view of the degradation kinetics. This lesser thermal stability appears due to the substitution of cyclopentyl groups with aliphatic *i*-butyl groups.

This finding seems to drive towards the use of CP-POSSs as nanofillers for POSSs based nanocomposites rather than towards that of hib-POSSs. Nevertheless, due to their low cost, these last compounds can be preferred if the temperatures during processing or in service are compatible with their thermal parameters, that are, in any case, quite good. We plan to study in the next future nanocomposites of PS and polyolefins with both series of POSSs.

References

1. Gupta RK, Kennel E, Kim KJ, editors. Polymer nanocomposites handbook. Boca Raton, FL: CRC Press Inc.; 2010.
2. Abate L, Blanco I, Bottino FA, Di Pasquale G, Fabbri E, Orestano A, Pollicino A. Kinetic study of the thermal degradation of PS/MMT nanocomposites prepared with imidazolium surfactants. J Therm Anal Calorim. 2008;91(3):681–6.
3. Olewnik E, Garman K, Czerwiński W. Thermal properties of new composites based on nanoclay, polyethylene and polypropylene. J Therm Anal Calorim. 2010;101(1):323–9.
4. Lomakin SM, Dubnikova IL, Shchegolikhin AN, Zaikov GE, Kozlowski R, Kim GM, Michler GH. Thermal degradation and combustion behavior of the polyethylene/clay nanocomposite prepared by melt intercalation. J Therm Anal Calorim. 2008;94(3):719–26.
5. Zaitsev VS, Filimonov DS, Presnyakov IA, Gambino RJ, Chu B. Physical and chemical properties of magnetite and magnetite-polymer nanoparticles and their colloidal dispersions. J Colloid Interface Sci. 1999;212:49–57.
6. Haraguchi K, Farnworth R, Ohbayashi A, Takehisa T. Compositional effects on mechanical properties of nanocomposite hydrogels composed of poly (N,N-dimethylacrylamide) and clay. Macromolecules. 2003;36:5732–41.
7. Hu Y, Chen JF, Zhang HT, Li TW, Xue X. Using silicon dioxide nanosphere gaps to confine growth of single-crystal nickel sulfide nanowires in polyacrylamide gel. Scripta Mater. 2006;55:131–4.
8. Yu SL, Zuo XT, Bao RL, Xu X, Wang J, Xu J. Effect of SiO_2 nanoparticle addition on the characteristics of a new organic-inorganic hybrid membrane. Polymer. 2009;50:553–9.
9. Chrissafis K, Paraskevopoulos KM, Tsiaoussis I, Bikiaris D. Comparative study of the effect of different nanoparticles on the mechanical properties, permeability, and thermal degradation mechanism of HDPE. J Appl Polym Sci. 2009;112:1606–18.
10. Avella M, Cosco S, Di Lorenzo ML, Di Pace E, Errico ME. Influence of $CaCO_3$ nanoparticles shape on thermal and crystallization behavior of isotactic polypropylene based nanocomposites. J Therm Anal Calorim. 2005;80(1):131–6.
11. Jiao C, Chen X. Synergistic effects of zinc oxide with layered double hydroxides in EVA/LDH composites. J Therm Anal Calorim. 2009;98(3):813–8.
12. Ramezanzadeh B, Attar MM, Farzam M. Effect of ZnO nanoparticles on the thermal and mechanical properties of epoxy-based nanocomposite. J Therm Anal Calorim. 2011;103(2):731–9.
13. Viratyaporn W, Lehman RL. Effect of nanoparticles on the thermal stability of PMMA nanocomposites prepared by in situ bulk polymerization. J Therm Anal Calorim. 2011;103(1):267–73.
14. Hu S, Hu Y, Song L, Lu H. Effect of modified organic-inorganic hybrid materials on thermal properties of cotton fabrics. J Therm Anal Calorim. 2011;103(2):423–7.
15. Fina A, Tabuani D, Frache A, Camino G. Polypropylene–polyhedral oligomeric silsesquioxanes (POSS) nanocomposites. Polymer. 2005;46:7855–66.
16. Weickmann H, Delto R, Thomann R, Brenn R, Döll W, Mülhaupt R. PMMA nanocomposites and gradient materials prepared by means of polysilsesquioxane (POSS) self-assembly. J Mater Sci. 2007;42(1):87–92.
17. dellErba IE, Williams RJJ. Epoxy networks modified by multifunctional polyhedral oligomeric silsesquioxanes (POSS) containing amine groups. J Therm Anal Calorim. 2008;93(1):95–100.
18. Villanueva M, Martín-Iglesias JL, Rodríguez-Añón JA, Proupín-Castiñeiras J. Thermal study of an epoxy system DGEBA (n = 0)/mXDA modified with POSS. J Therm Anal Calorim. 2009;96(2):575–82.
19. Wang XT, Yang YK, Yang ZF, Zhou XP, Liao YG, Lv CC, Chang FC, Xie XL. Thermal properties and liquid crystallinity of side-chain azobenzene copolymer containing pendant polyhedral oligomeric silsequioxanes. J Therm Anal Calorim. 2010;102(2):739–44.
20. Fina A, Monticelli O, Camino G. POSS-based hybrids by melt/reactive blending. J Mater Chem. 2010;20:9297–305.
21. Wang X, Wu L, Li J. Preparation of nano poly(phenylsilsesquioxane) spheres and the influence of nano-PPSQ on the thermal stability of poly(methyl methacrylate). J Therm Anal Calorim. doi:10.1007/s10973-011-1619-1.
22. Harrison PG. Silicate cages: precursors to new materials. J Organomet Chem. 1997;542(2):141–83.
23. Baney RH, Itoh M, Sakakibara A, Suzuki T. Silsesquioxanes. Chem Rev. 1995;95(5):1409–30.
24. Bolln C, Tsuchida A, Frey H, Mulhaupt R. Thermal properties of the homologous series of 8-fold alkyl-substituted octasilsesquioxanes. Chem Mater. 1997;9(6):1475–9.
25. Mantz RA, Jones PF, Chaffee KP, Lichtenhan JD, Gilman JW. Thermolysis of polyhedral oligomeric silsesquioxane (POSS) macromers and POSS–siloxane copolymers. Chem Mater. 1996;8(6):1250–9.
26. Fina A, Tabuani D, Frache A, Boccaleri E, Camino G. In: Le Bras M, Wilkie C, Bourbigot S, editors. Fire retardancy of polymers: new applications of mineral fillers. Cambridge: Royal Society of Chemistry; 2005. p. 202–20.
27. Fina A, Tabuani D, Carniato F, Frache A, Boccaleri E, Camino G. Polyhedral oligomeric silsesquioxanes (POSS) thermal degradation. Thermochim Acta. 2006;440(1):36–42.
28. Blanco I, Abate L, Bottino FA, Bottino P, Chiacchio MA. Thermal degradation of differently substituted cyclopentyl polyhedral oligomeric silsesquioxane (CP-POSS) nanoparticles. J Therm Anal Calorim. doi:10.1007/s10973-011-1848-3.
29. De Armitt C, Wheeler P. POSS keeps high temperature plastics flowing. Plastics Addit Compound. 2008;10(4):36–9.
30. Lee JY, Fu GC. Room-temperature Hiyama cross-couplings of arylsilanes with alkyl bromides and iodides. J Am Chem Soc. 2003;125(19):5616–7.

31. Murata M, Ishikura M, Nagata M, Watanabe S, Masuda Y. Rhodium (I)-catalyzed silylation of aryl halides with triethoxysilane: practical synthetic route to aryltriethoxysilanes. Org Lett. 2002;4(11):1843–5.
32. Weber WP. Silicon reagents for organic synthesis. Berlin, New York: Springer-Verlag; 1983.
33. Manoso AS, Ahn C, Soheili A, Handy CJ, Correia R, Seganish WM, Deshong P. Improved synthesis of aryltrialkoxysilanes via treatment of aryl grignard or lithium reagents with tetraalkyl orthosilicates. J Org Chem. 2004;69(24):8305–14.
34. Lichtenhan JD, Schwab JJ, Reinerth W, Carr MJ, An YZ, Feher FJ. Process for the formation of polyhedral oligomeric silsesquioxanes. US Patent WO 01/10871 A1.
35. Shimadzu DTG-60/60H Instruction manual. Shimadzu Corporation, Analytical & Measuring Instruments Division. Kyoto, Japan 2000.
36. User's manual TA 3000 System. Greifensee: Mettler Instr., AG, 1984.
37. Della Gatta G, Richardson MJ, Sarge SM, Stølen S. Standards, calibration, and guidelines in microcalorimetry. Part 2. Calibration standards for differential scanning calorimetry (IUPAC Technical Report). Pure Appl Chem. 2006;78(7):1455–76.